Electronic Supplementary Material (ESI) for Sustainable Energy & Fuels.

Supporting Information for

Impacts of Metal Oxide Additives on the Capacity and Stability of Calcium Oxide based Materials for the Reactive Sorption of CO_2

Luke T. Minardi[‡], *Faisal H. Alshafei*[‡,1], *Zubin K. Mishra, Dante A. Simonetti*[*]

Chemical and Biomolecular Engineering Department, University of California-Los Angeles, Los Angeles, CA 90095 (USA)

[1] Current Address: Division of Chemistry and Chemical Engineering, California Institute of Technology, Pasadena, CA 91125 (USA)

‡ Luke T. Minardi and Faisal H. Alshafei contributed equally

* Corresponding Author. Phone: 310-267-0169. Email: dasimonetti@ucla.edu

Theoretical Capacity Calculations:

The maximum theoretical capacities of the modified sorbents were calculated based on the mass fraction of CaO present in each sorbent. The sorbent notation is xM-yCa-O, where x is the moles of metal additive, y is the moles of Ca, and M is the identity of the metal additive. Assuming no CaO is consumed as a mixed oxide, mass fraction is determined by molar loadings and and the oxidation state of the additive oxide, using equation 1 below:

$$Mass\ Fraction\ CaO = \frac{yMW_{CaO}}{(yMW_{CaO} + \frac{x}{a}MW_{MOx})} \quad (1)$$

Where MW indicates the molecular mass of the oxide, x and y are the moles of M and Ca respectively (quantified by ICP-MS), and a is the stoichiometric factor from M_aO_b.

For samples containing aluminum, cobalt, chromium, gallium, and indium, mixed oxide species were identified via XRD, see below. The presence of the mixed oxide requires a correction to the mass fraction of CaO that can react with CO_2. The exact quantity of CaO consumed as a mixed oxide is not precisely known, therefore a lower bound of CaO present in the sample can be estimated by assuming all of the additive metal exists as a stoichiometric metal oxide using equation 2 below:

$$Mass\ Fraction\ CaO = \frac{(y - x(\frac{q}{r}))MW_{CaO}}{(yMW_{CaO} + \frac{x}{r}MW_{MixedOx})} \quad (2)$$

Stoichiometric factors of the mixed oxide q and r, for the oxide $Ca_qM_rO_s$, can account for the consumption of CaO and account for the mass of total mixed oxide. If no mixed oxide is formed, q=0 and r can be replaced with a, yeilding the same equation as used for separate oxide phases.

Maximum theoretical capacity of each sorbent may be calculated by multiplying the mass fraction of CaO, calculated via equation 1, and the stoichiometric capacity of CaO, C_{CaO} = 0.79 $g_{CO2}\ g_{CaO}^{-1}$ using equation 3. The corrected theoretical capacity is also caluclated using equation 3, but the mass fraction of CaO is calculated via equation 2.

$$C_{Sorbent} = C_{CaO} \times Mass\ Fraction\ CaO \quad (3)$$

For samples where a mixed oxide was identified both maximum theoretical capacity and corrected theoretical capacity were calculated by equation 3, so that upper and lower bounds of sorbent capacity could be estimated. The maximum theoretical capacity, upper bound estimate, is known to be inaccurate, as the mixed oxide has been confirmed. The lower bound estimate could potentially be inaccurate if less than 100% of the additive existed as $Ca_qM_rO_s$. Although there maybe inaccuracies with either bound, it is the simplist method for reasonable theoretical capacity estimates.

Morphological Discussion of Supplemental Information SEMs:

Figure S1 includes the SEM images not included in the main text for 3Co-10Ca-O, 3Cr-10Ca-O, 3In-10Ca-O, 3La-10Ca-O, 1Mg-2Ca-O, and 3Ga-10Ca-O. The same trends are observed for these samples as were discussed in the main text. The underperforming samples in **Figure S1**, in terms of capacity and stability, are 3Co-10Ca-O and 3Cr-10Ca-O. Both of these samples are higly agglomerated in their pre-cycle SEMs, it is also notable that the sample containing cobalt is very smooth and appears to have little surface texture. After cycling the particles size becomes much larger. Samples with maximum capacity greater than 0.40 g_{CO2} $g_{Sorbent}^{-1}$, 3La-10Ca-O and 1Mg-2Ca-O, are both highly textured, have small particle size and have high porosity. These samples improved stability compared to CaO, but they were ultimatley still not highly stable. This behavior is reflected in the post cycle SEMs. Significant particle growth can be seen for both samples, although they still retain some surface texture.
Middle performing samples, in terms of capacity and stability, 3In-10Ca-O and 3Ga-10Ca-O are also included in **Figure S1**. The fresh 3In-10Ca-O sample has the most unique texture. The particles are fairly smooth and are a mixture of spherical and nanorod geometries. The post-cycle 3In-10Ca-O sample also underwent particle growth and agglomeration, but some smaller particulates and nanorods can also be observed around these larger particles. The post-cycle 3Ga-10Ca-O sample is low resolution, but it can be seen that the particles are higly agglomerated and little porosity is visible. Overall, the moderate stability samples 3In-10Ca-O, 3La-10Ca-O, 1Mg-2Ca-O, and 3Ga-10Ca-O, have morphological changes similar to the unstable samples and they show significantly more agglomeration than the highly stable samples discussed in the main text.

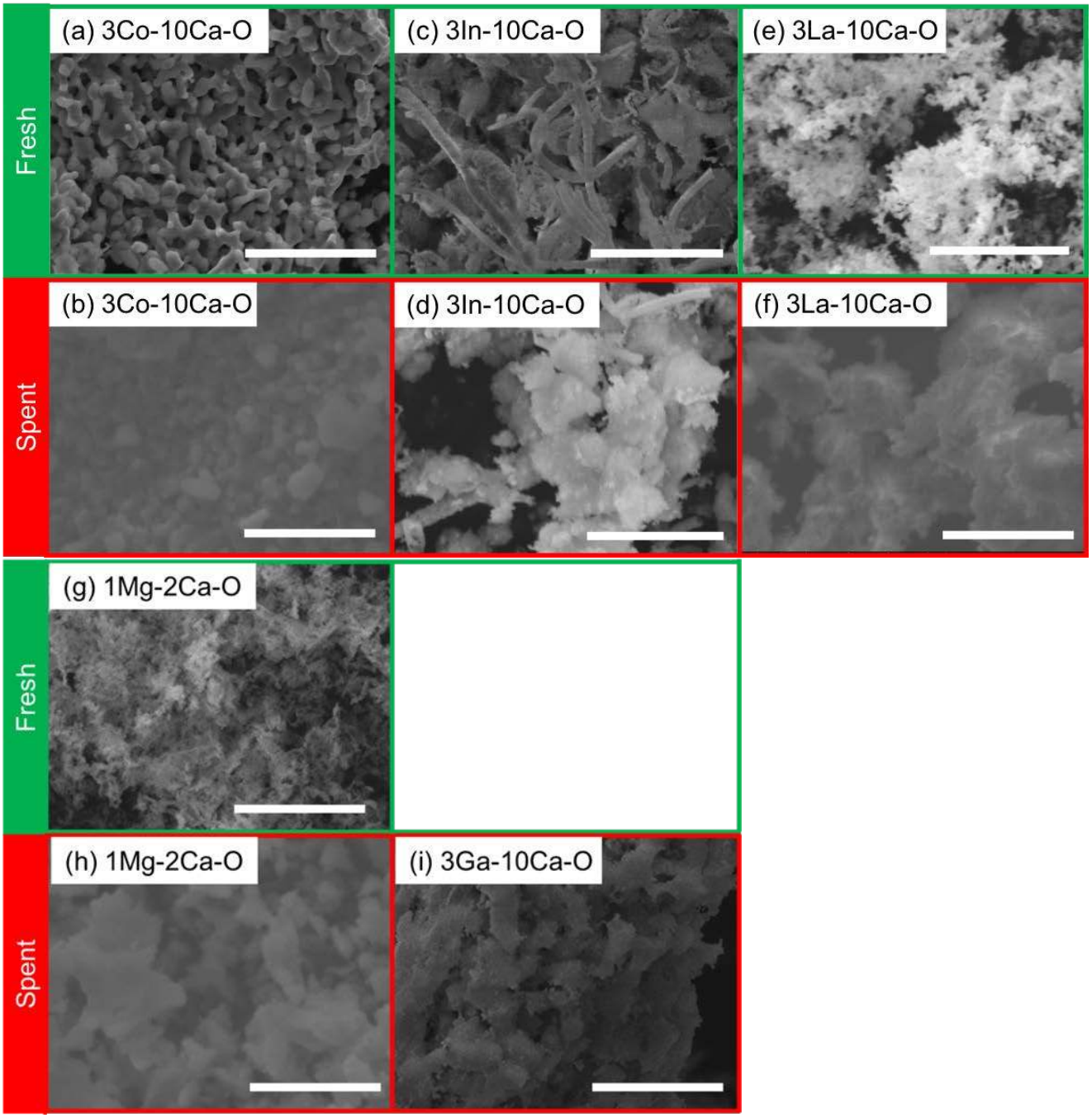

Figure S1. SEM images of (a) 3Co-10Ca-O fresh, (b) 3Co-10Ca-O post 11 cycles, (c) 3In-10Ca-O fresh,(d) 3In-10Ca-O post 16 cycles, (e) 3La-10Ca-O fresh, (f) 3La-10Ca-O post 11 cycles,(g) 1Mg-2Ca-O fresh,(h) 1Mg-2Ca-O post 16 cycles, (i) 3Ga-10Ca-O post 16 cycles. Samples bordered with green are fresh, samples bordered in red are post cycle samples, the white scale bar represents 5µm.

Identification of Metal Oxides in this Study and their Tammann Temperatures:

The identity of the metals present in the sorbents tested were identified via XRD, the peaks used for their identification is listed in **Table S1**. Peak identification can be seen on individual XRD spectra, before and after cycling, immediately following the table in **Figure S2a-n**.

Tammann temperature of the additive metal oxides present in this study are listed in **Table S1**. Samples such as 3Co-10Ca-O, 3Ga-10Ca-O, and 3In-10Ca-O were confirmed to have mixed oxides $Ca_3Co_2O_6$, $Ca_5Ga_6O_{14}$, and $CaIn_2O_4$ via XRD, but the Tammann temperature of the mixed oxides could not be found in literature. In these cases, the Tammann temperature of the additive metal oxide CoO, Ga_2O_3, and In_2O_3 was included instead. Tammann temperature was included for the metal oxide and mixed oxide was included for samples containing aluminum and chromium because they were readily avaible for both materials. Tammann temperature of the additive oxide was found to have a strong effect on both the maximum conversion and the stability, in terms of the first order deactivation constant, of sorbents tested. This is because if the metal oxide Tammann temperature is lower than the maximum treatment temperature the metal oxide will become agglomerated and lose its favoarble nanofibrous structure. Further, each regeneration occurs at high temperature, 1173 K, the higher the metal oxide Tammann temperatrue, less agglomeration was observed after carbonation-regeneration cycling.

Table S1. Melting-point, Tammann temperature, and XRD peak location that was used in Scherrer's equation as described in the main text. Compounds that do not have a Tammann temperature in the literature are reported as 50% of the melting point.

Compound	Melting Point (K)	Tammann Temperature (K)	XRD Peak Location (°)
CaO	3171	1586 [1–3]	37
MgO	3125	1461 [1–3]	43
Y_2O_3	2683	1473 [4]	48
Er_2O_3	2617	1309	29
Nd_2O_3	2506	1253	31
La_2O_3	2490	1286 [4]	30
Al_2O_3	2273	1263 [1–3]	N/A
ZnO	2248	983 [3,5]	36
In_2O_3	2183	1092	N/A
Ga_2O_3	2173	1087	N/A
CoO	2103	1052 [2,3]	N/A
Li_2O	1711	856	N/A
Cr_2O_3	2708	1354	N/A
$Ca_{12}Al_{14}O_{33}$	1688	844[6]	30
$CaIn_2O_4$	N/A	N/A	33
$Ca_5Ga_4O_{14}$	N/A	N/A	16
$Ca_3Co_2O_6$	N/A	N/A	46
$CaCrO_4$	2980	1490	25
$CaCO_3$	1612	806 [2,3]	N/A

X-ray diffraction raw data and peak identificaiton:

XRD scans were taken of samples before and after carbonation cycling. The pre-carbonation cycling scan and post-carbonation cycling scan are presented together on the same figure so that any changes in crystal structure can be identified.

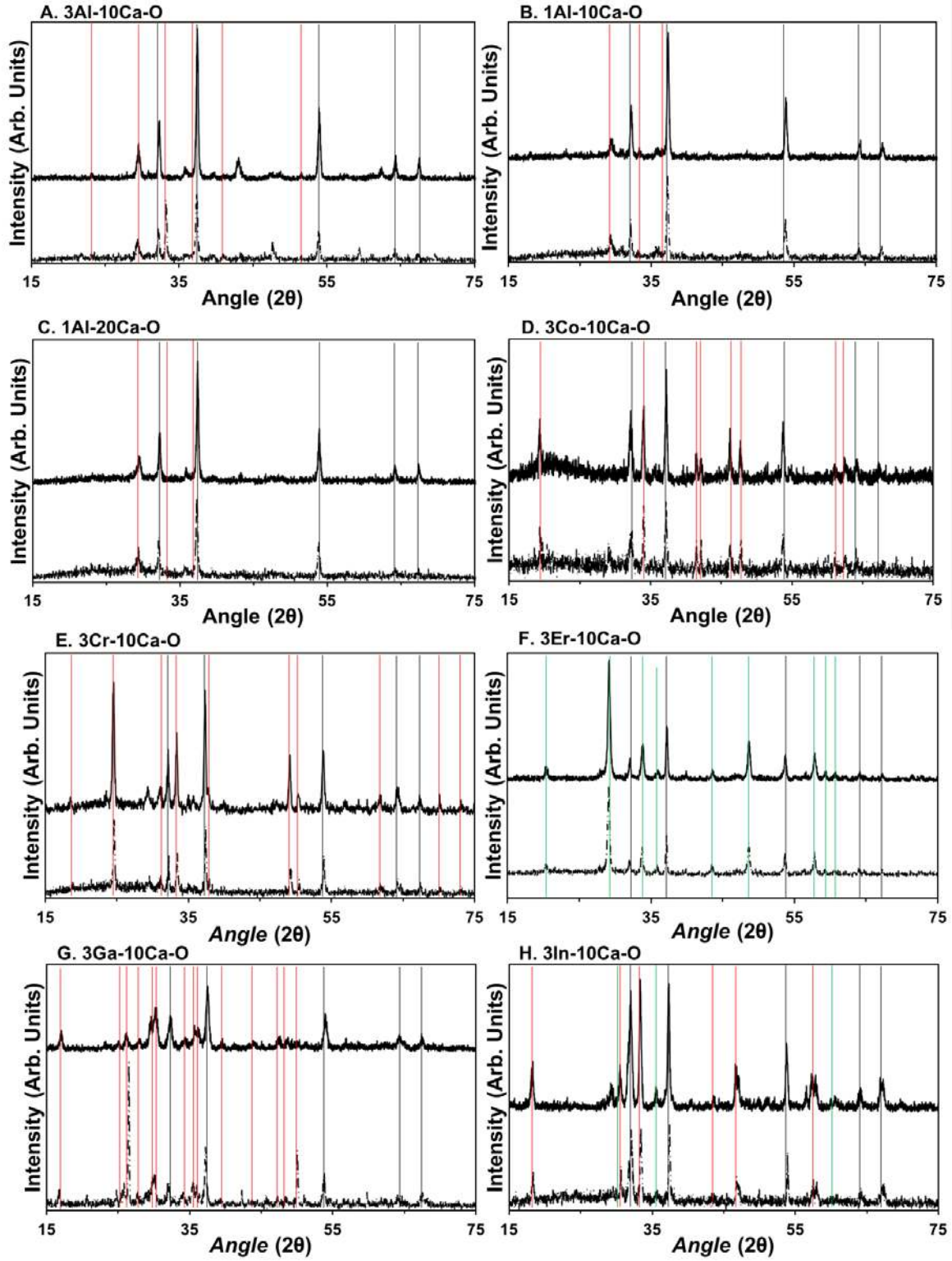

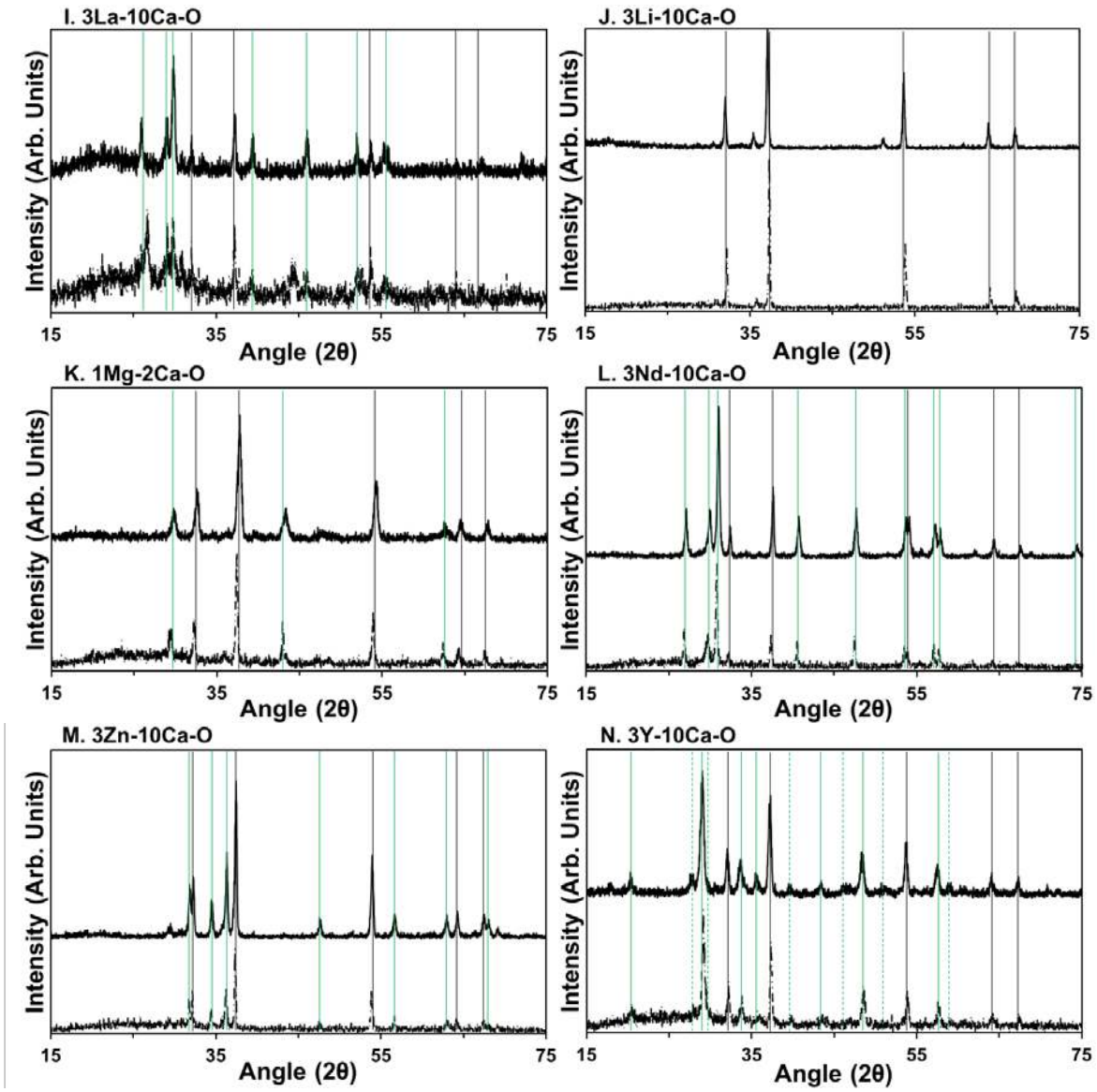

Figure S2. XRD spectra for A. 3Al-10Ca-O, B. 1Al-10Ca-O, C. 1Al-20Ca-O, D. 3Co-10Ca-O, E. 3Cr-10Ca-O, F. 3Er-10Ca-O, G. 3In-10Ca-O, H. 3Ga-10Ca-O, I. 3La-10Ca-O, J. 3Li-10Ca-O, K. 1Mg-2Ca-O, L. 3Nd-10Ca-O, M. 3Y-10Ca-O, and N. 3Zn-10Ca-O sorbents with the pre-cycle spectrum on top (solid line), and the post- cycle sample below (dashed line). Characteristic peaks for each crystal are identified using verticle lines: black lines indicate CaO (PDF#48-1467) characteristic peaks, green lines indicate the characteristic peaks for the metal oxide (M_xO_y), red lines indicate the characteristic peak for the mixed oxide ($Ca_xM_yO_z$). Yttrium hydroxide peaks were identified and labeled with green dashed lines.

Raw Data for TGA Carbonation-Regeneration:

Raw data for carbonation and regeneration steps for each cycle are presented below. Data for temperature ramps and holding steps for equilibrated temperature were eliminated for ease of analysis. Samples were initially exposed ot N_2 at 1073 K to ensure pure oxide. The sample was then cooled to 873 K, and exposed to CO_2 which resulted in the increase of sample mass observed below. Following carbonation, there is a temperature ramp (not shown). The mass loss corresponds to the TGA holding temperature at 1073 K in N_2.

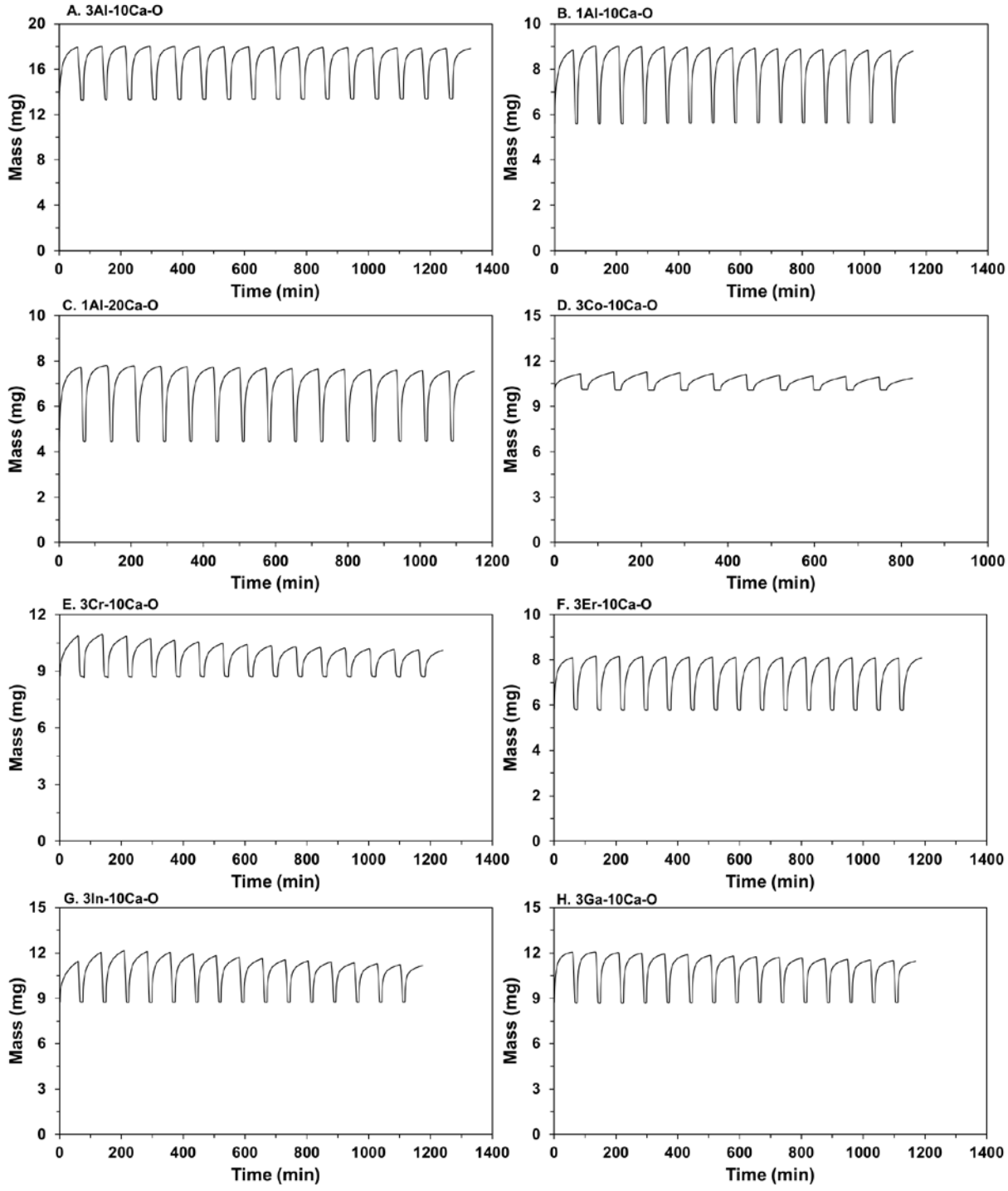

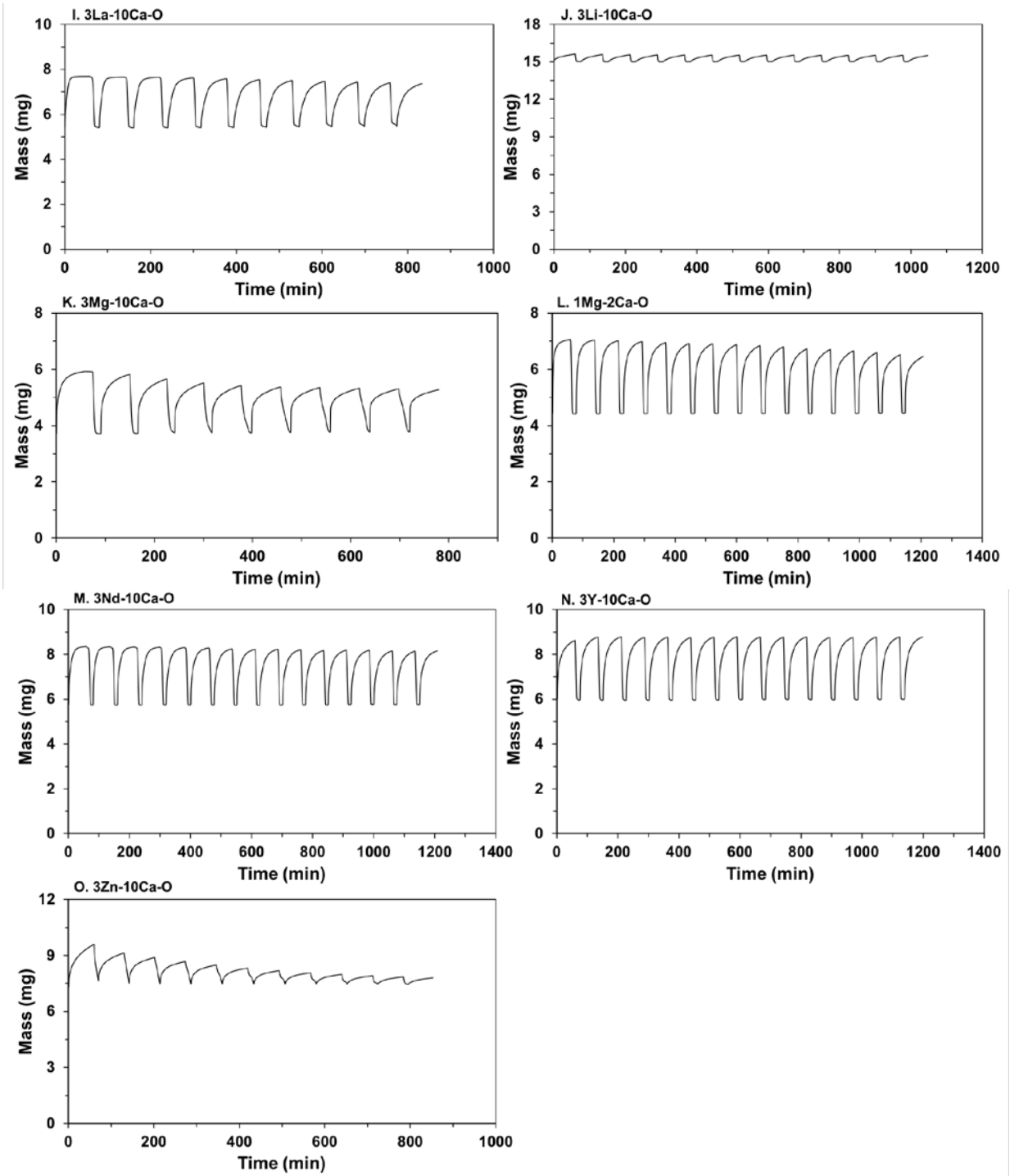

Figure S3. Raw data for TGA carbonation-regeneration cycling for A. 3Al-10Ca-O, B. 1Al-10Ca-O, C. 1Al-20Ca-O, D. 3Co-10Ca-O, E. 3Cr-10Ca-O, F. 3Er-10Ca-O, G. 3In-10Ca-O, H. 3Ga-10Ca-O, I. 3La-10Ca-O, J. 3Li-10Ca-O, K. 3Mg-10Ca-O, L. 1Mg-2Ca-O, M. 3Nd-10Ca-O, N. 3Y-10Ca-O, and O. 3Zn-10Ca-O sorbents. Each carbonation was carried out for 60 minutes in 200 sccm of 100% CO_2 at 873 K. Regeneration was carried out under 200 sccm of air at 1073 K for 10 minutes. Data is simplified by deleting data from temperature ramps and incubation periods to equilibrate sample temperature.

Random Pore Model Fit of First Carbonation:

The random pore model (RPM) shown in the main text was used to estimate a kinetic and diffusive rate parameter for CaO carbonation. A comparison of the RPM model fit to the raw data is seen in the figures below, where the solid line is the model fit and the hollow circles are the raw data for conversion as a function of time. The Y-axis is the conversion multiplied by the ratio of the theoretical capacity of mixed oxide and pure CaO samples.

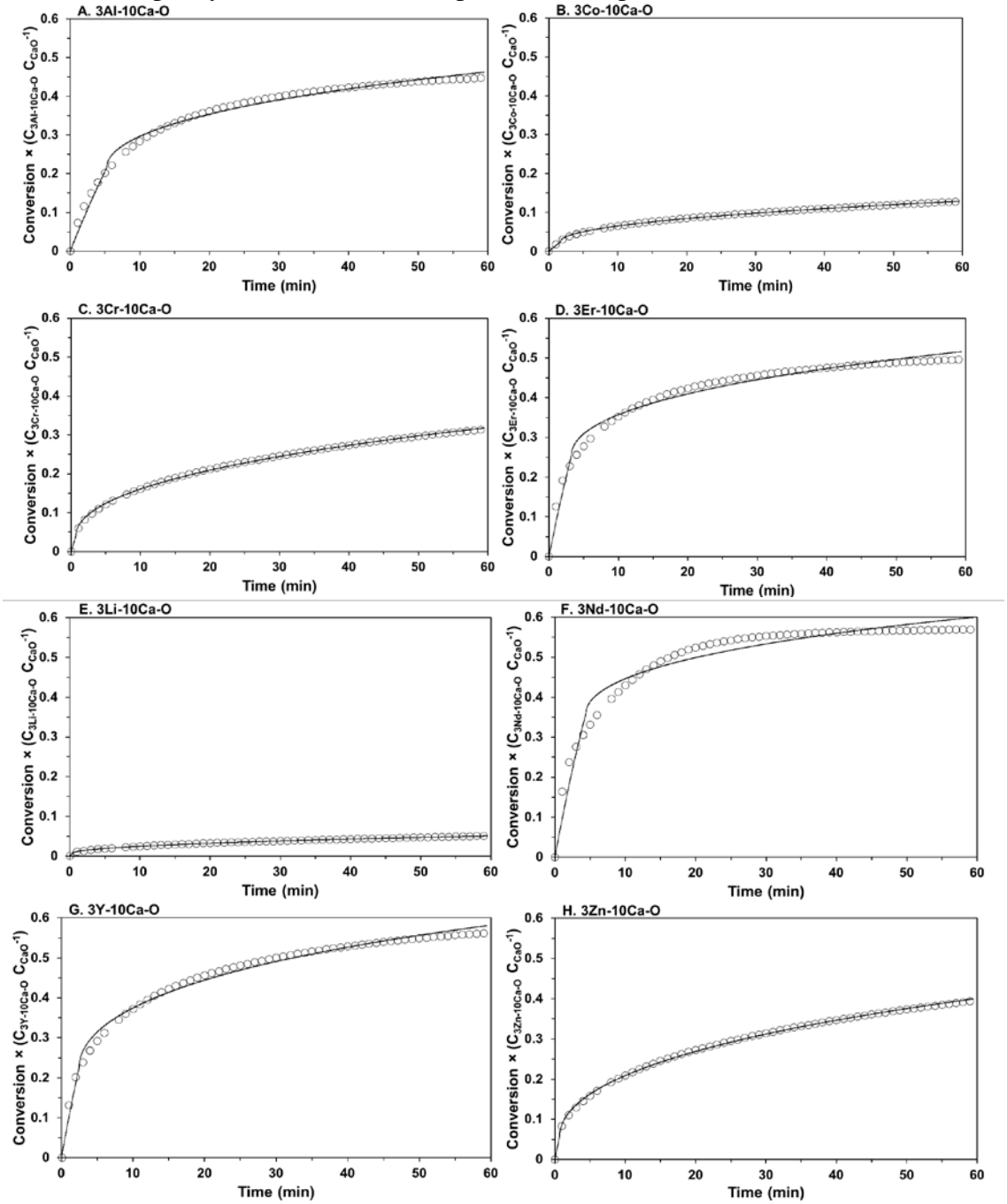

Figure S4. Raw data of the first carbonation (hollow circles) of A. 3Al-10Ca-O, B. 3Co-10Ca-O, C. 3Cr-10Ca-O, D. 3Er-10Ca-O, E. 3Li-10Ca-O, F. 3Nd-10Ca-O, G. 3Y-10Ca-O, H. 3Zn-10Ca-O sorbents with the optimized RPM fit used to determine k_{RPM} and D_{RPM} parameters. The experiment was carried out at in 200 sccm of 10% CO_2 at 873 K for 1 hr.

References

1 S. Tian, J. Jiang, F. Yan, K. Li and X. Chen, *Environ. Sci. Technol.*, 2015, **49**, 7464–7472.

2 J. Phromprasit, J. Powell and S. Assabumrungrat, *Chem. Eng. J.*, 2016, **284**, 1212–1223.

3 Y. Xu, C. Luo, Y. Zheng, H. Ding, Q. Wang, Q. Shen, X. Li and L. Zhang, *RSC Adv.*, 2016, **6**, 79285–79296.

4 Y. Xu, C. Luo, Y. Zheng, H. Ding, Q. Wang, Q. Shen, X. Li and L. Zhang, *RSC Adv.*, 2016, **6**, 79285–79296.

5 C. Doornkamp, M. Clement and V. Ponec, *J. Catal.*, 1999, **182**, 390–399.

6 A. M. Kierzkowska, R. Pacciani and C. R. Müller, *ChemSusChem*, 2013, **6**, 1130–1148.